transmission. Hence, for high-symmetry crystals (zone axis parallel to z axis), and to a greater or lesser degree for crystals of a more general morphology, these zone-axis symmetries apply both to electron-microscope lattice images and to convergent-beam patterns under z-axis-symmetrical illumination, and so impact also on space-group determination by means of high-resolution electron microscopy (HREM). In CBED, these elements lead to *whole pattern* symmetries, to which every point in the pattern contributes, regardless of diffraction order and Laue zone (encompassing ZOLZ and HOLZ reflections).

II. Reciprocity-induced symmetries, on the other hand, depend upon ray paths and path reversal, and in the present context have relevance only to the diffraction pattern. Crystal-inverting or horizontal crystal symmetry elements combine with reciprocity to yield *indirect* pattern symmetries lacking a one-to-one real-space correspondence, within individual diffraction discs or between disc pairs. Type II elements are assumed to lie on the central plane of the crystal, midway between surfaces, as symmetry operators; this assumption amounts to a 'central plane' approximation, which has a very general validity in space-group-determination work (Goodman, 1984*a*).

A minimal summary of basic theoretical points, otherwise found in Chapter 5.2 and numerous referenced articles, is given here.

For a specific zero-layer diffraction order $g\ (= h, k)$ the incident and diffracted vectors are $\mathbf{k}_0$ and $\mathbf{k}_g$. Then the three-dimensional vector $\mathbf{K}_{0g} = \frac{1}{2}(\mathbf{k}_0 + \mathbf{k}_g)$ has the pattern-space projection, $\mathbf{K}_g = {}^{p}[\mathbf{K}_{0g}]$. The point $\mathbf{K}_g = \mathbf{0}$ gives the *symmetrical Bragg condition* for the associated diffraction disc, and $\mathbf{K}_g \neq \mathbf{0}$ is identifiable with the angular deviation of $\mathbf{K}_{0g}$ from the vertical z axis in three-dimensional space (see Fig. 2.5.3.1). $\mathbf{K}_g = \mathbf{0}$ also defines the symmetry centre within the two-dimensional disc diagram (Fig. 2.5.3.2); namely, the intersection of the lines S and G, given by the trace of excitation error, $\mathbf{K}_g = \mathbf{0}$, and the perpendicular line directed towards the reciprocal-space origin, respectively. To be definitive it is necessary to index diffracted amplitudes relating to a fixed crystal thickness and wavelength, with both crystallographic and momentum coordinates, as $\mathbf{u}_{g,K}$, to handle the continuous variation of $\mathbf{u}_g$ (for a particular diffraction order), with angles of incidence as determined by $\mathbf{k}_0$, and registered in the diffraction plane as the projection of $\mathbf{K}_{0g}$.

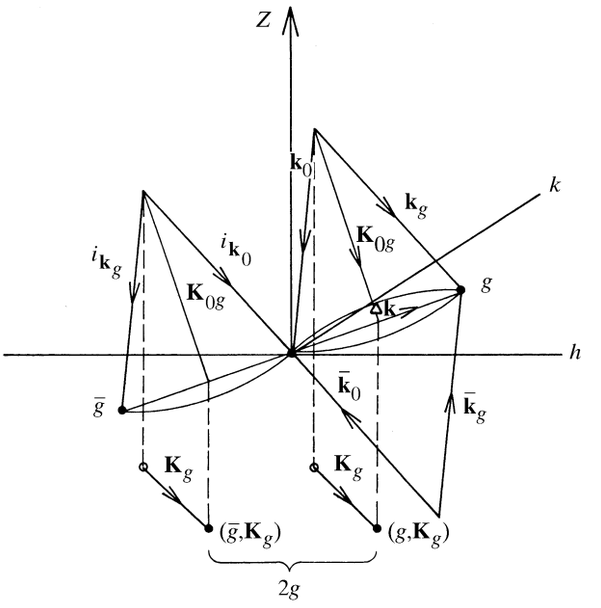

Fig. 2.5.3.1. Vector diagram in semi-reciprocal space, using Ewald-sphere constructions to show the 'incident', 'reciprocity' and 'reciprocity × centrosymmetry' sets of vectors. Dashed lines connect the full vectors $\mathbf{K}_{0g}$ to their projections $\mathbf{K}_g$ in the plane of observation.

2.5.3.2.2. *Reciprocity and Friedel's law*

Reciprocity was introduced into the subject of electron diffraction in stages, the essential theoretical basis, through Schrödinger's equation, being given by Bilhorn *et al.* (1964), and the N-beam diffraction applications being derived successively by von Laue (1935), Cowley (1969), Pogany & Turner (1968), Moodie (1972), Buxton *et al.* (1976), and Gunning & Goodman (1992).

Reciprocity represents a reverse-incidence configuration reached with the reversed wavevectors $\bar{\mathbf{k}}_0 = -\mathbf{k}_g$ and $\bar{\mathbf{k}}_g = -\mathbf{k}_0$, so that the scattering vector $\Delta\mathbf{k} = \mathbf{k}_g - \mathbf{k}_0 = \bar{\mathbf{k}}_0 - \bar{\mathbf{k}}_g$ is unchanged, but $\bar{\mathbf{K}}_{0g} = \frac{1}{2}(\bar{\mathbf{k}}_0 + \bar{\mathbf{k}}_g)$ is changed in sign and hence reversed (Moodie, 1972). The reciprocity equation,

$$\mathbf{u}_{g,\mathbf{K}} = \mathbf{u}^{*}_{g,\bar{\mathbf{K}}}, \tag{2.5.3.1}$$

is valid independently of crystal symmetry, but cannot contribute symmetry to the pattern unless a crystal-inverting symmetry element is present (since $\bar{\mathbf{K}}$ belongs to a reversed wavevector). The simplest case is centrosymmetry, which permits the right-hand side of (2.5.3.1) to be complex-conjugated giving the useful CBED pattern equation

$$\mathbf{u}_{g,\mathbf{K}} = \mathbf{u}_{\bar{g},\mathbf{K}}. \tag{2.5.3.2}$$

Since $\mathbf{K}$ is common to both sides there is a point-by-point identity between the related distributions, separated by $2g$ (the distance between g and $\bar{g}$ reflections). This invites an obvious analogy with *Friedel's law*, $F_g = F^{*}_{\bar{g}}$, with the reservation that (2.5.3.2) holds only for centrosymmetric crystals. This condition (2.5.3.2) constitutes what has become known as the $\pm H$ symmetry and, incidentally, is the only reciprocity-induced symmetry so general as to not depend upon a disc symmetry-point or line, nor on a particular zone axis (*i.e.* it is not a point symmetry but a translational symmetry of the pattern intensity).

2.5.3.2.3. *In-disc symmetries*

(*a*) *Dark-field (diffracted-beam) discs*. Other reciprocity-generated symmetries which are available for experimental observation relate to a single (zero-layer) disc and its origin $\mathbf{K}_g = \mathbf{0}$, and are summarized here by reference to Fig. 2.5.3.2, and given in operational detail in Table 2.5.3.2. The notation subscript R, for reciprocity-induced symmetries, introduced by Buxton *et al.* (1976) is now adopted (and referred to as BESR notation). Fig.

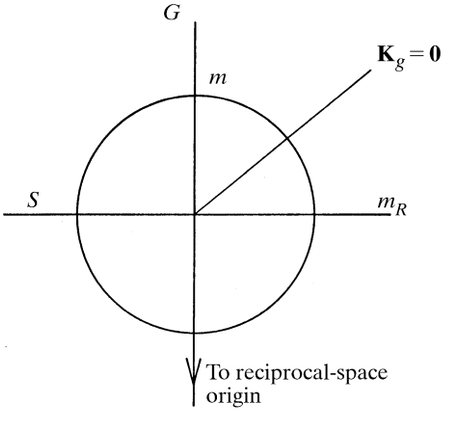

Fig. 2.5.3.2. Diagrammatic representation of a CBED disc with symmetry lines m, m_R (alternate labels G, S) and the central point $\mathbf{K}_g = 0$.

2.5.3.2 shows a disc crossed by reference lines m and m_R. These will be mirror lines of intensity if: (*a*) **g** is parallel to a vertical mirror plane; and (*b*) **g** is parallel to a horizontal diad axis, respectively. The third possible point symmetry, that of disc centrosymmetry (1_R in BESR notation) will arise from the presence of a horizontal mirror plane. Lines m and m_R become the GS extinction lines G and S when glide planes and screw axes are present instead of mirror planes and diad axes.

(*b*) *Bright-field (central-beam) disc*. The central beam is a special case since the point $\mathbf{K}_0 = \mathbf{0}$ is the centre of the whole pattern as well as of that particular disc. Therefore, both sets of rotational symmetry (types I and II) discussed above apply (see Table 2.5.3.3).

In addition, the central-beam disc is a source of three-dimensional lattice information from defect-line scattering. Given a sufficiently perfect crystal this fine-line structure overlays the more general intensity modulation, giving this disc a lower and more precisely recorded symmetry.

2.5.3.2.4. *Zero-layer absences*

Horizontal glides, a', n' (diperiodic, primed notation), generate zero-layer absent rows, or centring, rather than GS bands (see Fig. 2.5.3.3). This is an example of the projection approximation in its most universally held form, *i.e.* in application to absences. Other examples of this are: (*a*) appearance of both G and S extinction bands near their intersection irrespective of whether glide or screw axes are involved; and (*b*) suppression of the influence of vertical, non-primitive translations with respect to observations in the zero layer. It is generally assumed as a working rule that the zero-layer or ZOLZ pattern will have the rotational symmetry of the point-group component of the vertical screw axis (so that $2_1 \simeq 2$). Elements included in Table 2.5.3.1 on this pretext are given in parentheses. However, the presence of 2_1 rather than 2 (3_1 rather than 3 *etc.*) should be detectable as a departure from accurate twofold symmetry in the first-order-Laue-zone (FOLZ) reflection circle (depicted in Fig. 2.5.3.3). This has been observed in the cubic structure of $Ba_2Fe_2O_5Cl_2$, permitting the space groups $I23$ and $I2_13$ to be distinguished (Schwartzman *et al.*, 1996). A summary of all the symmetry components described in this section is given diagrammatically in Table 2.5.3.2.

2.5.3.3. *Pattern observation of individual symmetry elements*

The following guidelines, the result of accumulated experience from several laboratories, are given in an experimentally based sequence, and approximately in order of value and reliability.

(i) The value of X in an *X-fold rotation* axis is made immediately obvious in a zone-axis pattern, although a screw component is not detected in the pattern symmetry.

Roto-inversionary axes require special attention: $\bar{6}$ and $\bar{3}$ may be factorized, as in Tables 2.5.3.1, 2.5.3.3 and 2.5.3.4, to show better the additional CBED symmetries ($3/m'$ and $3 \times \bar{1}'$, respectively). $\bar{4}$ cannot be decomposed further (Table 2.5.3.1) and generates its own diffraction characteristics in non-projective patterns (see Section 2.5.3.5). This specific problem of observing the fourfold roto-

Table 2.5.3.2. *Diagrammatic illustrations of the actions of five types of symmetry elements (given in the last column in Volume A diagrammatic symbols) on an asymmetric pattern component, in relation to the centre of the pattern at* $\mathbf{K}_{00} = \mathbf{0}$*, shown as '* $\oplus$*', or in relation to the centre of a diffraction order at* $\mathbf{K}_{0g} = \mathbf{0}$*, shown as '+'*

Type	Symmetry element	Observation and action	In combination	Interpretation
Vertical	4			
	m; a	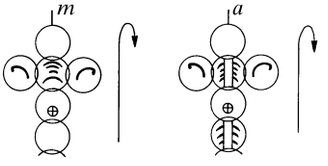	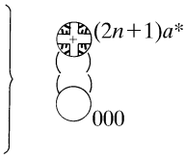	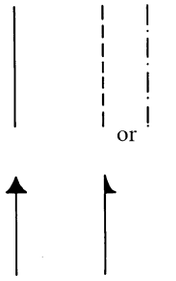
Horizontal	$2'$; $2'_1$	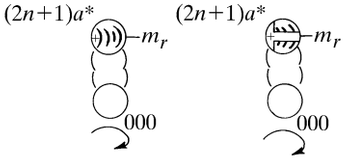		
	$i(\bar{1}')$	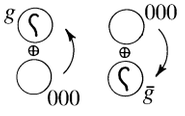		
	m'; a'	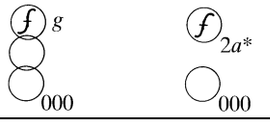		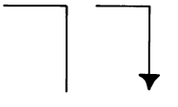

references